

Distinguishing Aerosol Impacts on Climate over the Past Century

DOROTHY KOCH

NASA Goddard Institute for Space Studies, Columbia University, New York, New York

SURABI MENON

Lawrence Berkeley National Laboratory, Berkeley, California

ANTHONY DEL GENIO

NASA Goddard Institute for Space Studies, Columbia University, New York, New York

RETO RUEDY

Sigma Space Partners, New York, New York

IGOR ALIENOV AND GAVIN A. SCHMIDT

NASA Goddard Institute for Space Studies, Columbia University, New York, New York

(Manuscript received 9 April 2008, in final form 29 August 2008)

ABSTRACT

Aerosol direct (DE), indirect (IE), and black carbon–snow albedo (BAE) effects on climate between 1890 and 1995 are compared using equilibrium aerosol–climate simulations in the Goddard Institute for Space Studies General Circulation Model coupled to a mixed layer ocean. Pairs of control (1890)–perturbation (1995) with successive aerosol effects allow isolation of each effect. The experiments are conducted both with and without concurrent changes in greenhouse gases (GHG). A new scheme allowing dependence of snow albedo on black carbon snow concentration is introduced. The fixed GHG experiments global surface air temperature (SAT) changed by -0.2° , -1.0° , and $+0.2^{\circ}\text{C}$ from the DE, IE, and BAE. Ice and snow cover increased 1% from the IE and decreased 0.3% from the BAE. These changes were a factor of 4 larger in the Arctic. Global cloud cover increased by 0.5% from the IE. Net aerosol cooling effects are about half as large as the GHG warming, and their combined climate effects are smaller than the sum of their individual effects. Increasing GHG did not affect the IE impact on cloud cover, however they decreased aerosol effects on SAT by 20%, and on snow/ice cover by 50%; they also obscure the BAE on snow/ice cover. Arctic snow, ice, cloud, and shortwave forcing changes occur mostly during summer–fall, but SAT, sea level pressure, and longwave forcing changes occur during winter. An explanation is that aerosols impact the cryosphere during the warm season but the associated SAT effect is delayed until winter.

1. Introduction

Atmospheric aerosols have multiple and complex impacts on climate. Distinguishing and quantifying these effects remains a major challenge of climate studies. The net effect of aerosol changes in the twentieth century on climate is thought to be cooling of surface air tempera-

tures (SAT), partially offsetting warming from increasing greenhouse gas (GHG) concentrations. However, some aerosol effects can contribute to warming. Furthermore, aerosols and GHG affect not only SAT, but also clouds and hydrology, and the cryosphere and atmospheric circulation. While the GHG changes affect these primarily via changes to the radiation–temperature, aerosols are thought to have additional “indirect” physical effects on clouds and cryosphere.

The best understood aerosol effect is the “direct” effect (DE), the scattering and absorption of radiation by aerosols suspended in the atmosphere. This effect cools

Corresponding author address: Dorothy Koch, NASA Goddard Institute for Space Studies, Columbia University, 2880 Broadway, New York, NY 10025.
E-mail: dkoch@giss.nasa.gov

the underlying surface, but if absorbing components are present, it can warm the local air mass. Although the DE is best understood, uncertainties remain in emissions, model transport and removal, aerosol microphysics such as chemical mixing and size distribution, and aerosol optical properties. Thus, the range in the DE change from preindustrial among recent aerosol models is -0.41 to $+0.04 \text{ W m}^{-2}$, with larger spread among individual aerosol species (Schulz et al. 2006). Black carbon (BC) absorption and warming within the air column can also cause shifts in cloud distribution. This has been called the semidirect effect and is included in models that have aerosol–radiation interaction.

Aerosols also increase cloud droplet number concentrations thereby increasing cloud albedo (first indirect effect); these are thought to reduce droplet size, suppress precipitation, increase cloud liquid water path and prolong cloud lifetime (second indirect effect). Since most clouds and pollution are low in the atmosphere, the overall effect is cooling. However, aerosol effects on ice clouds (e.g., Lohmann and Feichter 2005) and on Arctic clouds (Garrett and Zhao 2006; Lubin and Vogelmann 2006) are of uncertain sign.

Dark absorbing aerosols, especially BC, deposited on snow or ice surfaces can reduce the surface albedo, promote melting and therefore warm the climate. A simple parameterization of albedo reduction by BC deposition was developed by Hansen and Nazarenko (2004), and used in climate model studies (Hansen et al. 2005, 2007). Jacobson (2004) also included dependence of snow albedo and model radiation on BC snow concentrations. A sophisticated BC–snow model was developed by Flanner et al. (2007), who estimated a larger BC impact on albedo and greater efficacy (temperature change per forcing). The larger efficacy was attributed to the positive snow structure feedbacks within their scheme, or to differences among climate models.

We study aerosol effects in equilibrium coupled aerosol–climate experiments, for 1990s and 1890s conditions. To compare the aerosol effects, we perform a series of experiments, beginning with direct effects only, adding aerosol indirect effects (IE) on liquid clouds and finally BC–albedo (BAE) effects. Semidirect effects are included in all experiments, along with DE. Aerosol impacts may differ if GHGs change concurrently. Therefore we perform one set of experiments with only aerosol changes and a second with both GHG and aerosol changes.

There have been relatively few studies that include fully coupled aerosol–climate effects. Rotstayn and Penner (2001) simulated aerosol DE and IE using both fixed sea surface temperatures (SST) and equilibrium climate experiments and compared radiative forcing measures for these. Jacobson (2002) used a coupled aerosol–climate

model and compared warming effects of carbonaceous aerosols with that of GHG. Feichter et al. (2004) performed coupled aerosol DE and IE in equilibrium climate experiments and found the combined aerosol and GHG effects were reduced relative to the sum of the individual effects. In a BC–climate study, Wang (2004) found that BC has a significant effect on the model’s hydrologic cycle, generally slowing the hydrologic cycle and increasing low-level clouds. Jones et al. (2007) compared climate impacts from CO_2 with aerosol DE and IE. They found that anthropogenic BC and sulfate have comparable large high-latitude NH temperature response patterns, while CO_2 impacts high-latitude temperatures in both hemispheres, and biomass-burning aerosols cause a more uniform temperature response.

Since aerosols may have important effects on Arctic climate, we will include extra focus on this region. In a previous model study, Shindell (2007) showed that aerosol DE and IE on Arctic SAT are largest during winter, and suggested that this comes from nonlocal forcings. The study used the offline IE parameterization of Hansen et al. (2007) and did not include the effects of BC on snow albedo. We revisit the climate effects of aerosols within the Arctic using our fully coupled aerosol simulation.

2. Model description

We use Goddard Institute of Space Studies (GISS) ModelE (Schmidt et al. 2006) coupled to the aerosol simulation of sulfate, black and organic carbon, and sea salt (Koch et al. 2006, 2007). Model vertical resolution is 20 levels and horizontal resolution is $4^\circ \times 5^\circ$. Tracer mass, humidity, and heat are transported using the quadratic upstream scheme. Tracer dry deposition uses a resistance-in-series scheme; settling of aerosols is included. The aerosols, assumed to be externally mixed, affect model radiation as described in section 3b. Model cloud types are convective and stratiform, with a prognostic treatment of stratiform cloud water (Del Genio et al. 1996, 2005a). Aqueous sulfur chemistry and soluble species deposition are tightly coupled to the GISS model cloud schemes. Aerosol indirect effects on clouds are described in section 3c.

Simulated aerosol and precursor species include sulfate, sulfur dioxide (SO_2), hydrogen peroxide, dimethylsulfide, organic matter (OM), and black carbon (BC). Organic matter is assumed to include organic carbon (OC) and associated compounds, such that $\text{OM} = 1.3 \times \text{OC}$. Dry and aqueous sulfur chemistry are described in Koch et al. (2006, 1999). Sulfate and sea salt are assumed to be fully soluble within cloud droplets. Non-biomass-burning BC and OM are assumed to be emitted as insoluble, aging to soluble with e -fold lifetimes of 1 and 0.5 days,

respectively, to approximate the effect of mixing with soluble components. Biomass-burning BC and OM are assumed to have constant solubilities of 60% and 80%, respectively.

The model tracks aerosols after they are dry and wet deposited on and in snow. Snowpack resolution is 1–3 layers depending on snow thickness. Aerosols in snow are assumed to be fully soluble, so they are carried and removed by snowmelt, and may be carried to the base of the pack to be refrozen or to enter the ground layer below along with the water. We note that BC solubility in snow is uncertain but probably accumulates somewhat at the snow surface (e.g., Flanner et al. 2007), a feature we will incorporate in future studies.

We use aerosol emissions for mid 1990s and late 1890s. Sulfur emissions for 1995 anthropogenic sources are from the Emission Database for Global Atmospheric Research (EDGAR) v3.2 1995. Black and organic carbon anthropogenic emissions for the year 1996 are from Bond et al. (2004). Biomass-burning emissions for BC, OC, and SO₂ are based on the Global Fire Emissions Database (GFED v1; Koch et al. 2007). Natural SO₂ volcanic and DMS sources and natural OM emissions from terpenes are described in Koch et al. (2006). All emissions are injected into the lowest model level except for biomass burning, which is distributed across the model boundary layer (i.e., the level to which dry convection mixes) and volcanic emissions which are specified by the AeroCom model intercomparison project (more information available online at <http://nansen.ipsl.jussieu.fr/AEROCOM/>).

Emissions for 1890 SO₂ from energy generation are from van Aardenne et al. (2001). We derived our own 1890 carbonaceous aerosol emissions as follows. Carbonaceous fossil fuel emissions were assumed to come from coal combustion. The BC coal emissions are derived from the historic sulfur inventory of Lefohn et al. (1999), assuming 0.14 Tg BC (Tg S)⁻¹; OC emissions are assumed to be a factor of 4 larger than BC. Biofuel-burning history is taken from van Aardenne et al. (2001) SO₂ biofuel figures; the BC and OC biofuel emission is calculated using present-day ratios of biofuel BC and OC (from Bond et al. 2004) relative to the 1990 biofuel SO₂ emissions from van Aardenne et al. (2001). The resulting 1890 carbonaceous emissions are similar to those derived more precisely by Bond et al. (2007). For 1890 energy-production BC emission is 1.7 Tg yr⁻¹ compared with Bond et al.'s (2007) 2.0 Tg yr⁻¹; both emissions have 0.5, 0.8, 0.2 Tg yr⁻¹ from North America, Europe, and Southeast Asia, respectively. Total OC emission is 4.7 Tg yr⁻¹ (0.9, 1.6, and 0.8 Tg yr⁻¹ from North America, Europe, Southeast Asia) compared with Bond et al.'s (2007) 5.8 Tg yr⁻¹ (1.8, 1.8, and 0.5 Tg yr⁻¹

TABLE 1. Aerosol characteristics. Emissions are Tg S or C yr⁻¹. Burdens are Tg S, BC or OM; F_D = instantaneous TOA W m⁻², srf = surface, clr = clear TOA.

Species	Emissions	Burden	AOD × 100	F_D	srf F_D	clr F_D
1995						
Sulfate	106	0.40	5.3	-0.7	-0.7	-0.8
BC	8.2	0.19	0.38	0.5	-0.7	0.3
OM	59	1.2	1.9	-0.3	-0.7	-0.7
Total			7.6	-0.5	-2.1	-1.2
1890						
Sulfate	32	0.2	2.6	-0.4	-0.4	-0.5
BC	4.0	0.08	0.16	0.2	-0.3	0.1
OM	41	0.8	1.3	-0.2	-0.5	-0.5
Total			4.0	-0.4	-1.2	-0.9
1995–1890						
Sulfate	74	0.19	2.7	-0.3	-0.3	-0.3
BC	4.2	0.11	0.22	0.3	-0.4	0.2
OM	18	0.4	0.6	-0.1	-0.2	-0.2
Total			3.5	-0.1	-0.9	-0.3

from North America, Europe, and Southeast Asia). Little is known of historical biomass burning, so we assume the 1890 burning emissions were 0.5 present-day in tropical burning and African savanna regions but unchanged elsewhere. Natural emissions are assumed unchanged. Net emission for the species is in Table 1.

Model SO₂ and aerosols for 1995 are compared with observations in Koch et al. (2006, 2007). Model concentrations generally agree within a factor of 2 of surface concentration observations. The model ocean is a 65-m slab Qflux mixed layer. The mixed layer permits ocean response to atmospheric temperature change by adjusting energetically, rather than including the full ocean dynamics of a deep ocean. Schmidt et al. (2006) provides details of ModelE Qflux treatment. The model performances of fully dynamic and slab ocean are compared in Hansen et al. (2005, 2007). The climate sensitivity, 2.7°C for doubled CO₂ is the same for both ocean types; however the Southern Hemisphere warming is stronger for the Qflux slab ocean because it does not allow for deep ocean mixing and surface temperature moderation (Hansen et al. 2007). For the Qflux control simulations, the model net heat flux of energy into the ocean is adjusted to be close to zero. A 5-yr simulation is then performed, saving ocean horizontal heat transports and temperature at the base of the maximum mixed layer depth. These are applied as boundary conditions for the climate runs. The climate simulations are permitted to run until a steady SAT is achieved, and required 13–24 yr. The following 10 yr are analyzed. During these years the global mean SAT oscillates within 0.1°C; in the Arctic the mean SAT is also apparently steady but has larger variability, typically within 1.0°C.

TABLE 2. Equilibrium Qflux climate experiment definitions.

Experiment	Aerosols	GHG	Effects
D	1890	1990	Direct, control
	1995	1990	Direct, perturbation
DI	1890	1990	Direct and indirect, control
	1995	1990	Direct and indirect, perturbation
DIB	1890	1990	Direct, indirect, and BC-albedo, control
	1995	1990	Direct, indirect, and BC-albedo, perturbation
Dg	1890	1890	Direct, control
	1995	1990	Direct, perturbation
DIg	1890	1890	Direct and indirect, control
	1995	1990	Direct and indirect, perturbation
DIBg	1890	1890	Direct, indirect, and BC-albedo, control
	1995	1990	Direct, indirect, and BC-albedo, perturbation

We perform Qflux experimental pairs: control (1890) and perturbation (1995), listed in Table 2. Each successive pair includes an additional effect. The first set has only aerosol changes. The second set includes long-lived GHG changes, as well as changes in solar and ozone forcings. A third set of simulations used 1876–85 prescribed SSTs and 1890 GHG for purposes of calculating alternative aerosol forcing metrics.

3. Aerosol effects

a. Direct effects

For direct radiative effects, the aerosols are assumed to be externally mixed and the forcing calculations are based on Mie code embedded in the GCM (Schmidt et al. 2006). Effective radii (dry) are assumed to be 0.15, 0.2, and 0.09 μm for sulfate, organic carbon, and black carbon, respectively. These values are smaller than in our previous studies (e.g., Koch et al. 2007) in order to improve model comparison with retrieved Angstrom Exponent (Liu et al. 2006), Aerosol Robotic Network (AERONET) aerosol optical depth (AOD) and aerosol absorption optical depth. Otherwise, the aerosol optical properties are as described in Koch et al. (2007).

Global annual aerosol burden, AOD, instantaneous radiative forcing at the top of the atmosphere (TOA) and at the surface for 1995 and 1890 are in Table 1. These are given for the DE-only simulation; however, these results differ little among simulations. Annual mean AOD distributions for BC and sulfate are shown in Fig. 1. Sulfate AOD increases across the Northern Hemisphere (NH) between 1890 and 1995. BC also increases across most of the NH, however in the United Kingdom and in eastern United States, BC emissions and concentrations were larger in 1890. This negative change in BC is larger near the surface, as discussed below. Assumed biomass-burning changes have also increased the Southern Hemisphere (SH) BC burden. OC changes are roughly similar to those for BC. Global mean

sulfate and BC AODs approximately double over the century; however, OM forcing increases more modestly because of substantial and residential burning and natural sources in 1890.

The aerosol direct radiative forcing, F_D , is calculated from the difference between the TOA radiative flux with and without aerosols at each model time step (averaged for the month or year). We use the slab-ocean experiments for the calculation; however, the result is similar for the fixed SST ocean simulations (see section 5). The change in F_D from 1890 to 1995, the anthropogenic F_D or AF_D , is -0.1 W m^{-2} (Table 1; Fig. 2a). Table 1 also provides aerosol clear-sky F_D (last column), calculated by weighting F_D by the clear-sky fraction at each time step. The clear-sky AF_D is -0.3 W m^{-2} and is more negative than all-sky AF_D , because the scattering aerosol effect is greater when clouds are not the dominating source of scatter. Furthermore, BC positive forcing is larger when these absorbing aerosols overlie bright clouds (Haywood and Ramaswamy 1998; Penner et al. 1998), since they reduce the albedo. This more negative clear-sky forcing also occurs in other global aerosol models (Schulz et al. 2006). The AF_D at the model surface (Table 1; Fig. 2b) differs from the TOA forcing primarily because absorbing aerosols have a positive TOA forcing but negative surface forcing. The difference between TOA and surface forcing, or the atmospheric column forcing, doubles over the century from 0.8 to 1.6 W m^{-2} (Fig. 2c). The regions of strongest TOA negative forcing change (Fig. 2a) also generally have strongest column absorption (Fig. 2c), for example, the midlatitudes of the NH.

b. Indirect effect

Our aerosol indirect effect treatment includes the effects of aerosols on liquid-phase stratus and convective clouds. The impact is primarily on low-level stratus clouds, since these tend to be liquid and are in the vicinity of large

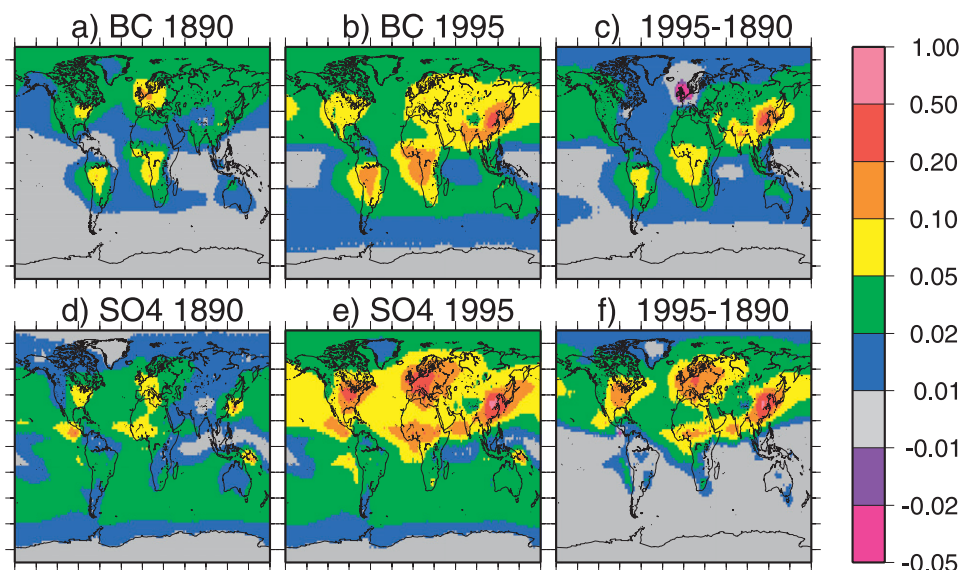


FIG. 1. Aerosol optical depths for BC ($\times 10$) in (a) 1890, (b) 1995, and (c) the change from 1890 to 1995; (d)–(f) for sulfate. Simulations DIB with all aerosol effects are used; however, other simulation pairs are similar.

aerosol concentrations. We use a semiprognotic relation between cloud droplet number concentration (CDNC) and aerosol number (converted from aerosol mass), based on observations (separate equations for convective and stratus clouds). For stratus clouds, CDNC depends also on cloud cover and turbulence where cloud-top entrainment stability is used as a proxy for in-cloud turbulence (Menon and Rotstajn 2006;

Menon et al. 2008). The autoconversion rate is based on a cloud droplet threshold size ($\sim 14 \mu\text{m}$; Menon and Rotstajn 2006). The IE simulation, in a similar version of the model, has been compared with several cloud microphysical variables from satellites [Moderate Resolution Imaging Spectroradiometer (MODIS), Advanced Microwave Scanning Radiometer for Earth Observing System (AMSR-E), Cloud and the Earth's Radiant

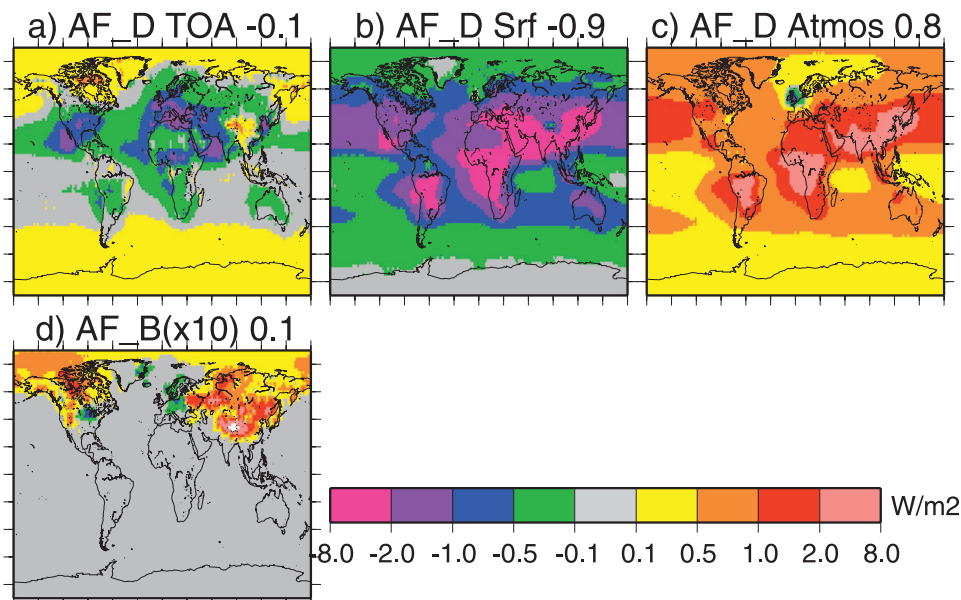


FIG. 2. Instantaneous radiative forcing change from 1890 to 1995 for net aerosol direct effect (a) at the TOA, (b) at the surface, and (c) in the column; (d) the BC-albedo instantaneous forcing change ($\times 10$); units are W m^{-2} .

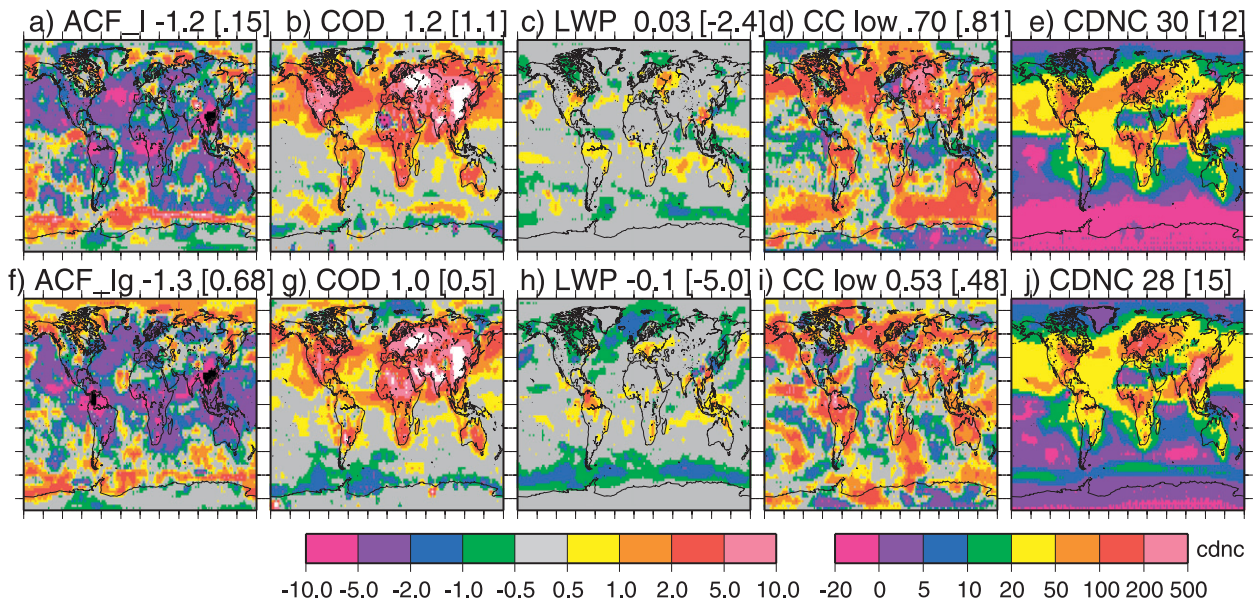


FIG. 3. Indirect effect diagnostic changes from 1890 to 1995 (top) for no GHG increase and (bottom) including GHG increase for (a),(f) ACF_I or net cloud forcing, $W m^{-2}$; (b),(g) warm stratus cloud optical depth; (c),(h) liquid water path, $kg m^{-2}$; (d),(i) low-level cloud cover, %; (e),(j) cloud droplet number concentration, cm^{-3} . Global (Arctic) average change is provided.

Energy System (CERES)]. Compared to observational constraints, the indirect effect was slightly overestimated for the Atlantic Ocean region (Menon et al. 2008) and thus, our estimates may be considered as an upper limit.

Figure 3 shows IE-related diagnostic changes from 1890 to 1995, where the top row is for the IE (DI-D) experiments and the bottom for the IE including GHG changes, Ig (DIg-Dg). One measure of the IE is the change in cloud forcing (CF) for different aerosol amounts. We define CF as the change in net, shortwave (SW) plus longwave (LW), TOA radiative flux, calculated as the instantaneous flux difference with and without clouds, then averaged monthly and annually. The “anthropogenic” change in cloud forcing from 1890 to 1995, ACF_I , is shown in Figs. 3a,f. The ACF_I is generally negative in polluted regions where the aerosol load is greatest. The CDNC (Figs. 3e,j) and cloud optical depth (COD; Figs. 3b,g) also increase in polluted regions. The cloud liquid water path (LWP; Figs. 3c,h) increases and precipitation decreases (not shown) over most land areas. Generally, the LWP increases (decreases) for low (high) latitudes from increased aerosols, and decreases (increases) for low (high) latitudes from GHG increase (not shown). A similar result was found by Jones et al. (2007), who argued that the LWP changes respond more to thermodynamic changes, such as the shift from ice to liquid phase clouds in a warming polar climate, rather than microphysical (IE) changes. As expected, low-level cloud cover (CC; Figs. 3d,i) increases overall.

The ACF_I depends on changes in both CC and LWP. Table 3 shows ACF for runs D, DI, and I, where ACF_I is the difference between ACF_{DI} and ACF_D . ACF_D is positive overall, especially over oceanic regions. This is because the CF for 1995 over oceans consists of the difference between dark aerosols over bright clouds (scene with cloud) and bright aerosols over dark oceans (scene without clouds), leading to a relatively positive CF compared with the preindustrial case. These effects are removed for the IE, and $ACF_I = -1.2 W m^{-2}$ or $ACF_{Ig} = -1.3 W m^{-2}$ (Figs. 3a,f). The global IE cloud forcing change thus does not change very much with GHG changes. As for the DE, these calculations were done with a slab ocean; however, the results are similar for fixed SST, as discussed further in section 5.

The ACF_I is negative in most regions and is maximum over Asia, where aerosol amount has increased most. The decrease in LWP near the Arctic apparently causes the positive ACF_I there, as well as in the Southern Ocean. This is not the longwave cloud effect described by Lubin and Vogelmann (2006) and Garrett and Zhao (2006). The positive Arctic ACF_I is in the shortwave and is maximum in summertime, especially beyond the periphery of the ice sheet where cloud changes have a larger impact on radiation.

c. BC-albedo effect

We have implemented a new model scheme for snow albedo dependence upon BC snow concentration. We first compared model BC air and snow concentrations

TABLE 3. Indirect effect forcing calculations. ACF = anthropogenic cloud forcing, ACF_g includes GHG increases, SST has fixed SST, AF is TOA flux change.

Case	D			DI			I		
	Net	SW	LW	Net	SW	LW	Net	SW	LW
Qflux ACF	0.55	0.48	0.07	-0.62	-0.41	-0.21	-1.17	-0.89	-0.28
Qflux ACF _g	0.86	1.39	-0.53	-0.44	-0.04	-0.41	-1.31	-1.43	0.12
SST ACF	0.62	0.63	-0.01	-0.62	-0.55	-0.07	-1.24	-1.18	-0.06
SST TOA AF	-0.16	-0.14	-0.02	-1.38	-1.47	0.09	-1.22	-1.33	0.11

and removal from the 1995 simulation with available recent Arctic observations. Removal is from dry and wet deposition, and the wet removal can be by either liquid or frozen precipitation. There is uncertainty in how much BC is removed by frozen precipitation. We found that 12% removal by ice, relative to liquid, gives optimal agreement with observations. This fraction is confirmed by observations during winter in Jungfraujoch by Cozic et al. (2007) who measured 60% removal of BC by liquid phase clouds and 5%–10% removal by mixed phase clouds, or 8%–17% removal by mixed phase relative to liquid phase; our 12% assumption falls midrange of these observations.

As shown in Koch et al. (2007), model BC surface concentrations agree to within 50% in Alaska (Denali and Barrow) and are underestimated but within a factor of 2 at Spitsbergen. Figure 4 shows three deposition features, observed and modeled. Figures 4a,b show deposited BC (ng/g) for annual average and the winter–spring months. The November–April time period is selected because most observations are from these months. BC transport to and removal within the Arctic are largest during this time. BC snow concentration data within the circles (Figs. 4a,b) are 1990s data cited within Flanner et al. (2007; Table 2). The model agreement with observations is within 10% in Greenland and Halifax, but model BC deposition is a factor of 2 too large in the Arctic Ocean (76°N, 165°E) and a factor of 10 too small in the Alps.

The fraction of particle removal by dry versus wet deposition in the Arctic is quite uncertain. Davidson et al. (1985) compared wet and dry removal at Dye 3 in Greenland. They estimated about 25% dry deposition for soluble species for annual average, but about 50% during the dryer spring months. The model agrees well at this location for the annual average and generally with the seasonality. Harder et al. (1996, their Fig. 2) showed that in Antarctica, wet deposition dominates if snow accumulation rate exceeds 15–20 g cm⁻² yr⁻¹. Since Arctic accumulation is observed to be within this range, about 16 g cm⁻² yr⁻¹ (Warren et al. 1999), we expect that dry deposition and wet deposition should be roughly equal. Model precipitation in the Arctic is about 13 g cm⁻² yr⁻¹, somewhat less than observed.

Model Arctic BC removal is generally more wet than dry (Fig. 4c), but dry and wet deposition are roughly equal during the dryer winter months (Fig. 4d). Another constraint is the scavenging ratio, or the fraction of aerosol within precipitation relative to that within air (Fig. 4e). Davidson et al. (1985) observed values of 100–200 for soluble species at Dye 3; Noone and Clarke (1988) measured about 100 in Abisko, Sweden. The model scavenging ratio agrees with the latter, and is smaller but within a factor of 2 at Dye 3.

The change in albedo as a function of BC snow concentration is taken from Warren and Wiscombe (1985, hereafter WW85; Fig. 2). We use the “spectrally averaged” albedo reduction in the figure because the model has only one visible snow-albedo band (300–770 nm); this band and the first near infrared (770–860 nm) are both reduced. WW85 provides albedo reduction for both fresh (0.1-mm grain radius) and old melting (1-mm grain size) snow. We derive snow grain size as a function of model SAT and snow age from Marshall (1989, illustrated in her Fig. 3.4 with FORTRAN code in Appendix B). We interpolate linearly between the 0.1- and 1-mm snow grain size curves (WW85; Fig. 2) to determine the albedo depression from BC snow concentration. BC concentrations in the top layer of land snow and snow on sea ice are used to determine the albedo reduction.

We measure the BAE radiative forcing F_B by taking the instantaneous difference between the TOA radiative flux with and without the BC–albedo effect for each radiation time step (averaged monthly and annually). For this calculation we used the fixed SST experiments. The global average 1995 F_B is 0.03 W m⁻², and difference between 1995 and 1890, ΔF_B is 0.01 W m⁻² (Fig. 2d). The Arctic ΔF_B is 0.03 W m⁻². These forcing changes are especially large near the major source region of south-central Eurasia. Snow cover within this region varies from 30% in winter to 2% in summer. Peak ΔF_B is over 4 W m⁻² in springtime when snow cover and solar angle combine to provide maximum forcing. The model of Flanner et al. (2007) also had maximum forcing in this region. Like the BC AOD change (Fig. 1c), the ΔF_B near Europe and eastern United States is negative since BC emissions were larger in 1890 than in 1995.

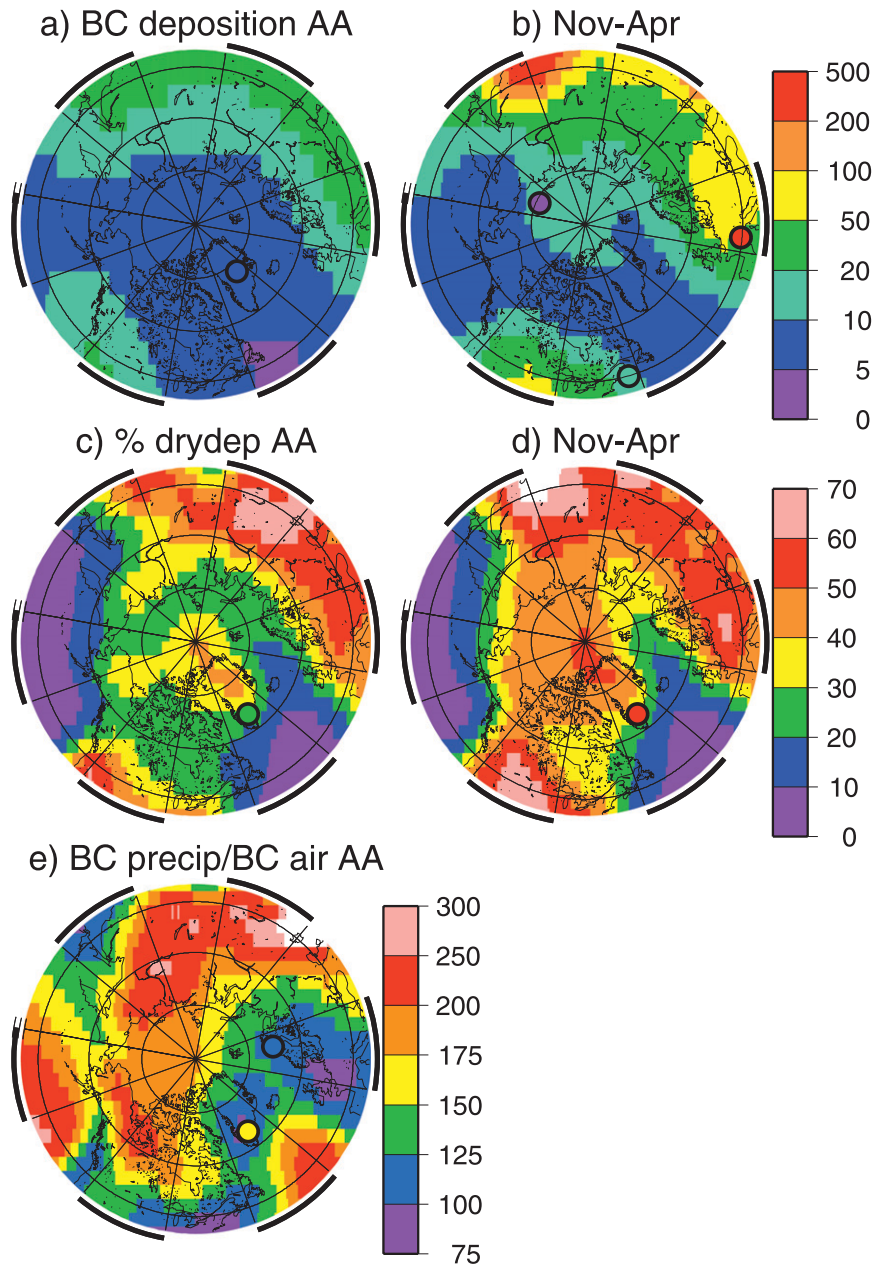


FIG. 4. Model BC deposition (ng BC/g precipitation) (a) annual average and (b) November–April; circles are observations referenced within Flanner et al. (2007). Model percent dry (relative to total) deposition: (c) annual average, and (d) November–April. Observations are from (c) Davidson et al. (1985) and (d) Noone and Clarke (1988). Annual average scavenging ratio (BC in precipitation/air); observations are from Davidson et al. (1985).

4. Climate responses

We now consider aerosol effects on climate in the Qflux experiments, including changes in surface temperature, clouds, and other hydrologic features, snow and ice cover, dynamics and radiative flux. We also seek correlations among these.

a. Surface air temperature

Figures 5a,b,c show the D, DI, and DIB (includes DE, IE, and BAE) experiments' effects on SAT. Although the aerosol–climate effects may not be exactly linear; that is, a given effect may differ when combined with other effects, we are better able to see them if we take the

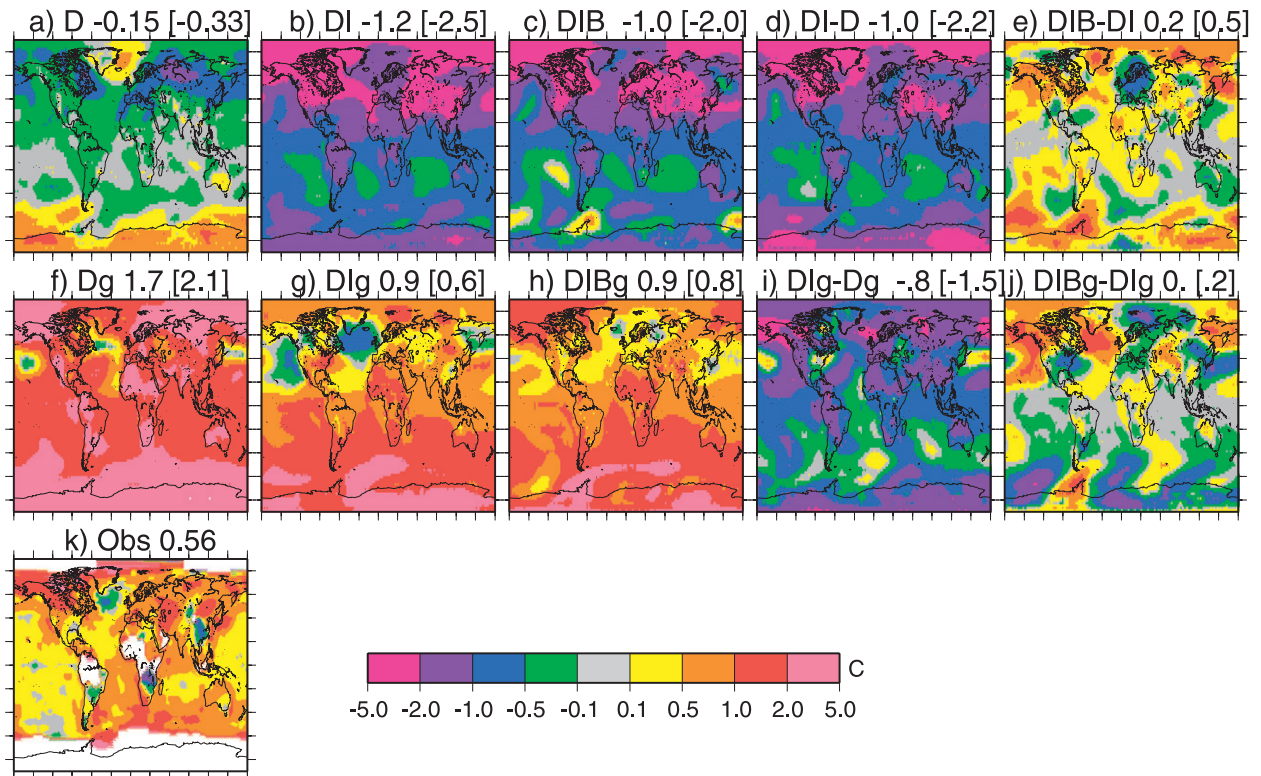


FIG. 5. Surface air temperature changes from 1890 to 1995 because of (a),(f) aerosol direct effects; (b),(g) indirect effects; and (c),(h) BC-albedo effect. Here we isolate (d),(i) the indirect effect [differences between (b) and (a), and (g) and (f), respectively] and (e),(j) the BC-albedo effect [differences between (c) and (b), and (h) and (g), respectively]. (top) Experiments without GHG changes and (second row) experiments include changing GHG. Global (Arctic, 64°–90°N) average change is provided. (k) Observed change from 1890 to 2000 from the GISS Surface Temperature Analysis (<http://data.giss.nasa.gov/gistemp/maps>); white indicates lack of long-term observations.

difference between successive experiments. Furthermore, Jones et al. (2007) demonstrated that aerosol DE and IE on SAT and precipitation are approximately additive in their model. Figure 5d shows the IE on SAT (difference between Figs. 5a and 5b) and Fig. 5e shows the BAE on SAT (difference between Figs. 5c and 5b).

The aerosol effects are clearest in the experiments with fixed GHG (top row). The DE lowers SAT by -0.15°C (Fig. 5a), with largest decreases over Eurasia. Increased temperature over Antarctica is due to increased SH biomass burning sending absorbing aerosols over the bright polar region. The IE lowers the temperature by another -1.0°C (Fig. 5d) and cooling increases with latitude, especially in the NH. The BAE raises the SAT slightly relative to the experiment without BAE, 0.18°C (Fig. 5e). This effect is also largest in polar regions, but cooling occurs over Europe because of the smaller 1995 BC in this region.

The GHG effect dominates the net SAT change (bottom row of Fig. 5). We cannot distinguish the DE from the GHG increase (Fig. 5f) because we have allowed both to change together. Nevertheless the aerosol

impact on SAT is evident over the northern oceans. For these experiments the IE (Fig. 5i) and BAE (Fig. 5j) on SAT are weaker than with fixed GHG.

Although we do not expect equilibrium Qflux slab-ocean experiments that do not include all relevant forcings to reproduce the temperature changes perfectly, we may compare with the observed SAT change from 1890 to 2000 (Fig. 5k). The simulation with all three aerosol effects and GHG changes (Fig. 5h) agrees best with the observed changes. Run DIBg average SAT increase is larger ($+0.9^{\circ}\text{C}$ instead of $+0.6^{\circ}\text{C}$), because our experiment is run to equilibrium; note also that the polar regions lack observational constraint, where model temperature increase is largest. The biggest discrepancy is in the Southern Oceans, where deep-ocean circulation would moderate the temperature change, and ice melt in the equilibrium experiment would exceed observations. However even in the historical transient GISS model simulation that included a deep ocean (Hansen et al. 2007), the SAT increase is more than observed in the Southern Ocean. Also, as in Hansen et al. (2007) model simulations, we lack sufficient warming over

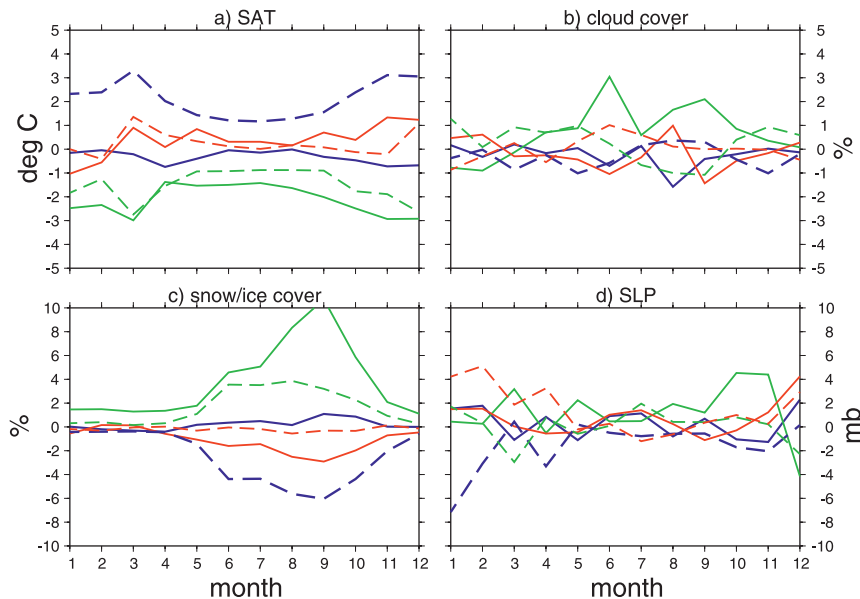


FIG. 6. Monthly Arctic changes (64° – 90° N) in (a) SAT, (b) cloud cover, (c) snow/ice cover, and (d) SLP for runs D (blue), Dg (blue dashed), DI-D (green), DIg-Dg (green dashed), DIB-DI (red), DIBg-DIg (red dashed).

Europe; this was attributed to excessive sulfate increase in that region. The model also fails to produce the observed cooling trends in Southeast Asia, southern Africa, and South America. These are regions where present-day model aerosol loads, and possibly emissions, may be underestimated. Compared with recent aerosol surface concentrations in Southeast Asia, the model is generally too small by more than a factor of 2 (Koch et al. 2007). The model African and South American regions may also have underestimated biomass-burning aerosols that would cool the underlying SAT. Biomass-burning trends are highly uncertain and our assumptions of their changes during the century are quite simple (see section 2). Apart from these discrepancies, many of the observed patterns are reproduced in the model, for example, with larger warming over continents and at high latitudes, and cooling south of Greenland.

The average Arctic (north of 60° N) SAT changes are given in brackets in Fig. 5. Typically the Arctic SAT change is approximately double the global average change. Seasonalities of these changes are in Fig. 6a. The maximum impacts on SAT occur during winter–spring.

b. Hydrologic effects

Climate model clouds typically shift when temperatures change. The GISS ModelE clouds have nearly neutral global climate feedback with doubled CO_2 (Schmidt et al. 2006); however, this is due to regionally compensating changes. Warmer temperatures increase low-level water vapor, and, as this is transported in up-

welling regimes to the upper troposphere, relative humidity and cloudiness increase aloft but decrease at low levels. Thus, at low-to-midlatitudes low-level cloudiness generally decreases (increases) in response to warmer (cooler) temperatures (Del Genio et al. 2005a, 2005b; Yao and Del Genio 1999). Such cloud changes provide positive temperature feedbacks; these feedbacks are balanced by negative cloud feedbacks in the polar regions for doubled CO_2 (Yao and Del Genio 1999). Figure 7 shows the percent change in cloud cover (CC) for the experiment pairs. The net cloud change is dominated by low-to-midlevel clouds.

Comparison of cloud (Fig. 7) with SAT (Fig. 5) changes suggests correlation between these in many regions. The DE simulations without GHG changes have increased clouds (Fig. 7a) over the same midlatitude NH regions that are cooler (Fig. 5a); the loss of clouds near Greenland may explain the warming there. The simulation with IE has increased low-level clouds over midlatitudes especially in the NH (Figs. 7b,d), consistent with cooling of the midlatitudes of the NH (Figs. 5b,d). Spatial cross correlations (dot product by model grid cell) between cloud and SAT changes are in Table 4. Correlation between SAT and cloud cover changes is -0.22 for DE and -0.33 for IE. For low cloud cover these are larger, -0.34 and -0.53 . The IE thus increases correlation between CC and SAT.

GHG warming decreases CC over midlatitudes of both hemispheres (Fig. 7f). The IE increases CC by 0.5% with or without GHG increase (Figs. 7d,i). The

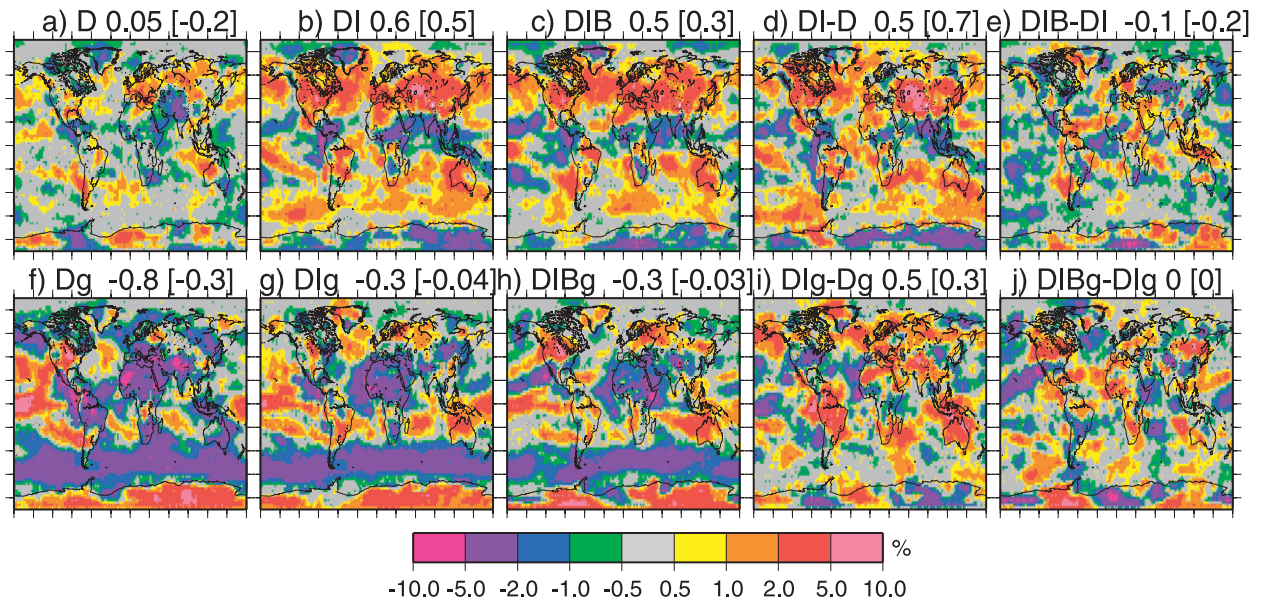


FIG. 7. Cloud cover (%) changes from 1890 to 1995 because of (a),(f) aerosol direct effects; (b),(g) indirect effects; (c),(h) BC–albedo effect. Here we isolate (d),(i) the indirect effect and (e),(j) the BC–albedo effect. (top) The experiments without GHG changes and (bottom) the experiments include changing GHG. Global (Arctic, 64°–90°N) average change is provided.

SAT and CC changes with IE and increased GHG (Figs. 5i, 7i) are more variable spatially than without GHG increases, since aerosols and GHG have opposing influences on CC. Nevertheless, the correlation between CC and SAT changes remains: cooler temperatures over the northern oceans correlate with increases in CC; warmer temperatures in the Pacific–Asian outflow region correlate with decreased CC there.

The BAE does not produce significant net CC changes. Nevertheless, the regional SAT changes typically correlate with CC changes. For example, cooling over Europe and the United States (Fig. 5e) is associated with increased clouds (Fig. 7e). Anticorrelation between CC and SAT changes within the Arctic are especially large for the DIBg run (Table 4, correlation of -0.4). Here there are increased clouds and reduced temperatures over Northern Europe, decreased clouds and warmer temperatures over the northern oceans.

We compare these cloud changes with those in similar GISS model simulations. Hansen et al. (2005)

prescribed a -1.0 W m^{-2} IE forcing by making the CC change dependent upon offline aerosol mass fields, and had 1.1% increased CC for fixed SST experiments. In the same model but in a transient 1880 to 2000 coupled ocean experiment, the CC increased by 0.8% (Hansen et al. 2007). Their parameterized IE caused larger CC changes than our online prognostic IE.

Global mean precipitation and evaporation decrease (increase) in response to decreased (increased) temperature changes in the experiments. Precipitation and evaporation both decrease by $-0.03 \text{ mm day}^{-1}$ from the DE (from 1890 to 1995) if GHG is fixed. They increase by 0.10 mm day^{-1} from the DE if GHG increases. Adding IE decreases precipitation and evaporation by $-0.07 \text{ mm day}^{-1}$ in both experimental pairs. Thus the aerosol effects nearly cancel the GHG effects on the global mean hydrologic system in our experiments. This is also seen in the full-ocean twentieth-century GISS model simulation (Romanou et al. 2007). The BAE has

TABLE 4. Correlations among global (Arctic) changes from 1890 to 1995. Dot product correlations among changes in fields; CLD = cloud cover, SNO/ICE = snow and ice cover.

Fields	D	DI	DIB	Dg	DIg	DIBg
CLD vs SAT	-0.22(-0.24)	-0.33(0.06)	-0.35(-0.06)	-0.27(-0.18)	-0.31(0.05)	-0.29(-0.42)
LOW CLD vs SAT	-0.34(-0.33)	-0.53(0.10)	-0.54(-0.07)	-0.41(-0.15)	-0.48(0.01)	-0.47(-0.45)
SAT vs SNO/ICE	-0.40(-0.46)	-0.48(-0.25)	-0.51(-0.37)	-0.32(-0.49)	-0.31(-0.31)	-0.33(-0.34)
CLD vs SNO/ICE	0.16(0.33)	0.32(0.44)	0.35(0.34)	0.13(0.22)	0.15(0.28)	0.21(0.27)
SLP vs SAT	0.22(-0.27)	-0.67(-0.40)	-0.55(-0.09)	-0.11(-0.21)	-0.31(-0.44)	-0.08(0.27)

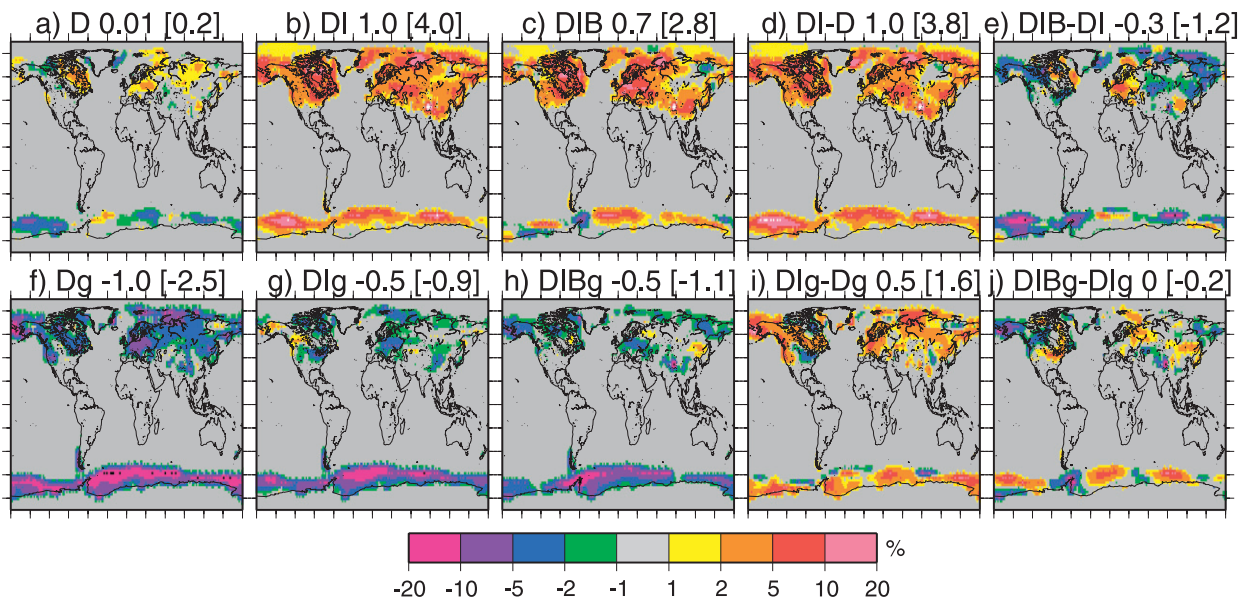


FIG. 8. As in Fig. 7, but for snow and ice cover (%) changes.

negligible global average effects on precipitation and evaporation.

The seasonality of Arctic CC changes is shown in Fig. 6b. The largest change is increased CC because of the IE (without GHG increase). This case had +0.7% cloud cover, maximum during summertime. Water vapor also decreased, primarily during summer.

c. Snow/ice/albedo

Aerosols impact snow and ice cover and therefore ground albedo in two ways. Their cooling effect on surface temperatures promotes ice and snow cover, raising ground albedo as the dark ground is covered with bright ice/snow. However, BC deposition darkens the snow, reduces surface albedo, and promotes melting of snow, which further decreases albedo. Figure 8 shows aerosol effects on snow/ice cover; impacts on ground albedo (not shown) are similar in sign and distribution.

Global snow/ice cover in the GISS model is about 10%. Thus, without GHG changes (Fig. 8, top row), cooling from the aerosol DE increases snow/ice cover by about 1% of the original cover (Fig. 8a). The IE cooling increases snow/ice by about 10% (Figs. 8b,d) and the BAE decreases snow/ice cover by about 3% (Figs. 8c,e), relative to the original cover. In western Europe the snow cover increases because of decreased BC emissions. The changes in ice/snow are anticorrelated with SAT changes, with cross correlations ranging from -0.4 to -0.5 (Table 4).

With GHG increase (Fig. 8, bottom), the warmer temperatures promote melting of snow/ice and therefore decrease albedo. The IE again increases ice/snow cover

(Fig. 8i), but the effect is smaller by a factor of 2 compared to the case without GHG change (Fig. 8i versus Fig. 8d). Thus the combined aerosol IE and GHG effects are smaller than the sum of their individual effects. The correlation between snow/ice cover and SAT changes are also smaller if GHGs increase (about -0.3 instead of -0.4 to -0.5). With the GHG increase, the change in ice/snow albedo from the BC-albedo effect is negligible globally (Fig. 8j). However, albedo/ice/snow are reduced in northwestern North America; they increase in eastern North America and much of Eurasia. Note the spatial correlation among these changes (Figs. 8i,j) and cloud changes (Figs. 7i,j) and SAT changes (Figs. 5i,j). In general, the cryospheric and cloud cover changes are positively correlated (Table 4) with cross correlations from 0.13 – 0.35 , and are generally larger in the Arctic.

The smaller impact of BAE on snow/ice with increased GHG results partly from increased BC removal rate from 1890 to 1990, so that more BC is removed near source regions and less is transported to the Arctic. The change from cooler to warmer climate causes a shift from ice to liquid phase clouds in the model: globally, GHG warming causes 1% increase in liquid and 1% decrease in ice phase clouds between 1890 and 1995. These shifts are reversed with fixed GHG as the climate is cooling. (A similar shift occurs in the Arctic as for the global average.) Since we assume that liquid clouds remove BC more effectively than ice clouds, the BC load, and Arctic deposition increase less in the simulation with GHG changes (Fig. 9b versus Fig. 9a). The smaller increase in BC in the Arctic reduces the impact of BC on snow/ice albedo.

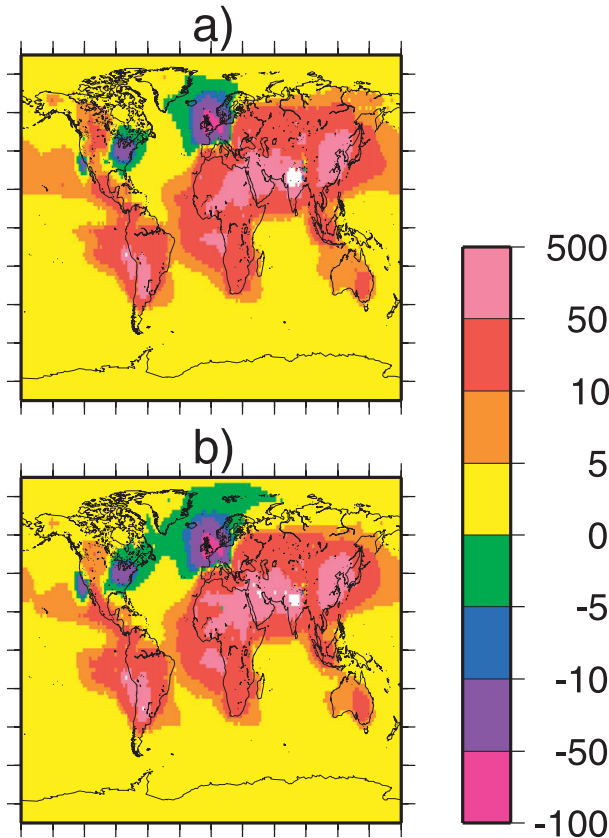


FIG. 9. Change in BC removal (ng BC/g precipitation) from 1995 to 1890 for (a) no change in GHG and (b) change in GHG.

Seasonality of Arctic snow/ice cover change is shown in Fig. 6c. Impacts are at a maximum during summer–fall. The largest effect is from the IE (without GHG change). Cross correlation of snow/ice and cloud cover is 0.44 (Table 4). The IE impact on snow/ice cover persists into the winter months. However, again these effects (Fig. 6c) are clearly not in phase with the SAT seasonality (Fig. 6a). As we will discuss further below, the SAT impacts may have delayed seasonal effect.

d. Dynamics

Aerosols also impact atmospheric circulation patterns. Figure 10 shows the changes in sea level pressure (SLP) and Fig. 11 the effects on zonal streamfunction. Some changes in SLP–circulation seem to be associated with warming–cooling of the overall climate. Many models (e.g., Hansen et al. 2007; Shindell et al. 1999; Proshutinsky and Johnson 1997; Hu and Wu 2004; Sigmund et al. 2004) but not all (see discussion in Rind et al. 2005) have a tendency for positive Arctic or North Atlantic Oscillation (AO/NAO) and decreased Arctic SLP with warmer climate. Various mechanisms may be responsible (Rind

et al. 2005), including warming of the tropics, reduction of equator–pole temperature gradient and change in refraction of planetary waves leading to a positive AO configuration. Consistent with this, our SAT (Fig. 5) and SLP (Fig. 10) changes are generally anticorrelated, especially in the NH, with cross correlations given in Table 4. (The DE has negative cross correlation in the NH, although positive in the SH.) Aerosol cooling from DE and IE have increased Arctic SLP (Figs. 10a,b,d) and reduced poleward low-level meridional velocity (Fig. 11a). Warming due to increased GHG reduces Arctic SLP (Fig. 10f) and enhances poleward velocity (Fig. 11f).

However, the BAE, a generally warming effect, has overall increased Arctic SLP (Figs. 10e,j) especially during wintertime (Fig. 6d, red curves), and the Arctic cross correlation of SLP with SAT (Table 4) is small or even positive (for increased GHG). Negative correlation does occur for BAE, just south of the Arctic, especially over the northern oceans. Also in the SH, the SLP and SAT are sometimes positively correlated over Antarctica, but negatively correlated over the oceans, for example, for DI, DIg, Dg. These support an ocean-temperature-driven mechanism for the SAT–SLP anticorrelation tendency.

The Arctic seasonality of SLP changes (Fig. 6d) are largest during winter, generally anticorrelating with the SAT changes, except for the BAE with its positive SAT–SLP correlation. This suggests larger dynamical effects during winter.

5. Discussion

Aerosol radiative forcing is often used to infer expected effects on temperature. Here we consider definitions of aerosol radiative forcing or flux change used by us and compare with estimates from other studies. We also use the SW and LW radiative flux changes in the Arctic as a tool to understand the aerosol climate impacts there.

We reported the 1890 to 1995 change of the TOA radiative flux change with and without the presence of aerosol DE (Table 1), clouds (the ACF; Table 3), and the BC effect on snow albedo (Fig. 2d). A possible difficulty with these diagnostics is that they involve taking the difference with the same atmosphere but without the forcing agent, an artificial state.

Several alternative definitions of radiative forcing have been explored in detail by Hansen et al. (2005). One measure that appears to provide an accurate indication of temperature impact and is relatively easy to calculate is the TOA radiative flux changes due to a changing forcing agent with SST held constant, F_s . This is especially useful for the second IE since the “forcing”

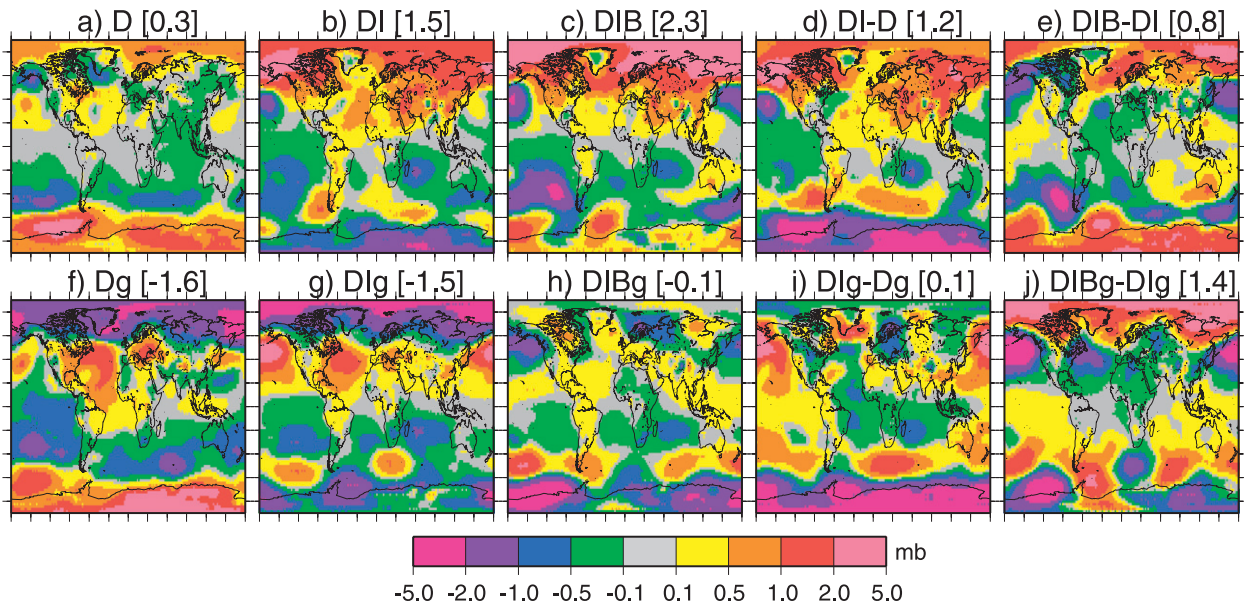


FIG. 10. As in Fig. 7, but for sea level pressure (mb) changes.

also includes a change in the forcing agent, cloud amount. This approach was first proposed and called “quasi-forcing” by Rotstayn and Penner (2001). It was altered by Hansen et al. (2005) by the addition of the (typically small) perturbation to the SAT, normalized by the model climate sensitivity, for the fixed SST ex-

periment. Rotstayn and Penner (2001) compared various estimates of aerosol forcing, by carefully defining experiments that isolated direct, first and second indirect aerosol effects. They demonstrated that quasi-forcing provides a good estimate of pure forcing, where pure forcing was the difference in TOA radiative flux

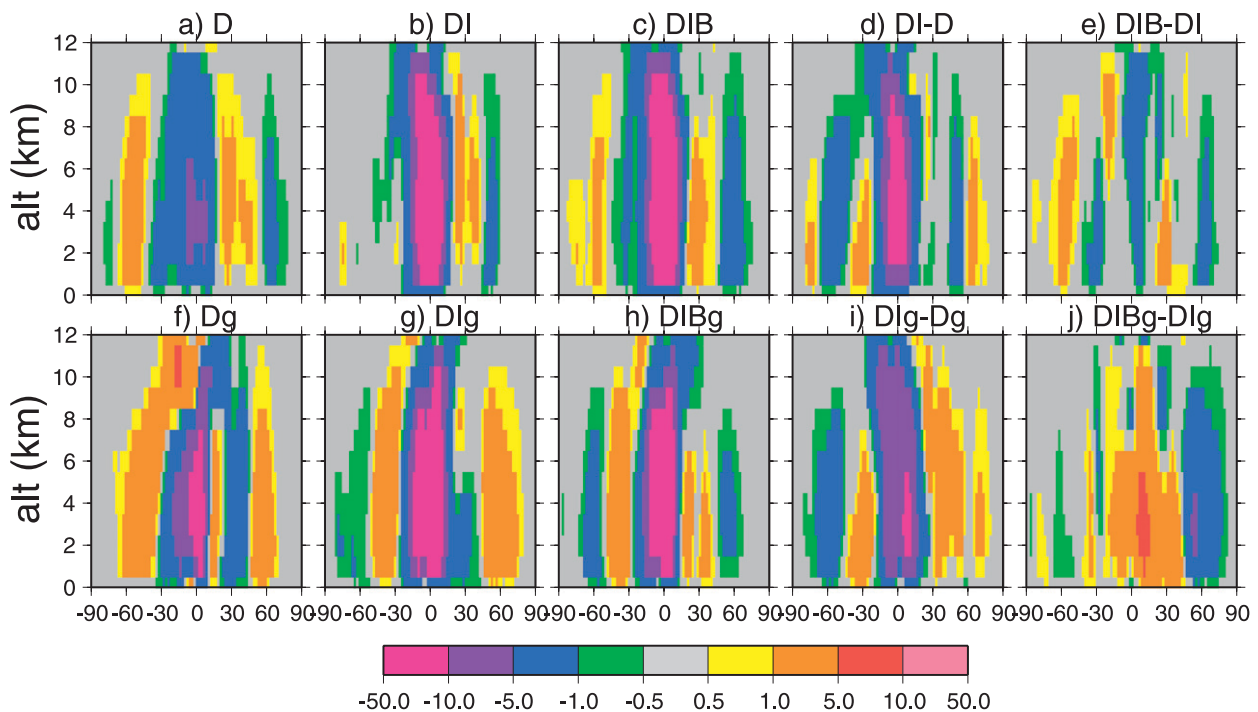


FIG. 11. As in Fig. 7, but for stream function ($\times 10^9 \text{ kg s}^{-1}$, positive = clockwise) changes.

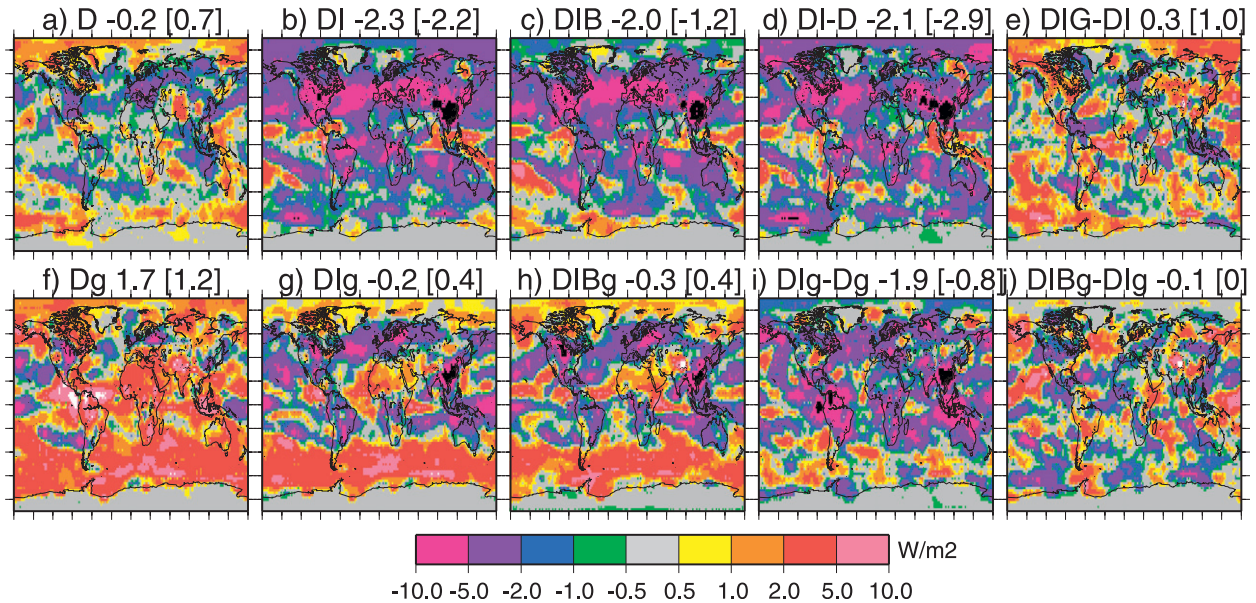


FIG. 12. As in Fig. 7, but for shortwave radiative forcing at the TOA (W m^{-2}) changes.

using present-day versus preindustrial forcing agents. Such a calculation could only be performed for DE and first IE. They also showed that the change in net TOA irradiance is nearly the same as the change in cloud forcing, for the first and second indirect effects, so that clear-sky feedbacks are small.

We consider similar questions here, although our experiments were not designed to isolate radiative flux changes apart from climate changes and atmospheric feedbacks. We note that, similar to Rotstajn and Penner (2001), the cloud forcing change ACF_7 is nearly identical to the change in TOA radiative flux AF_7 (Table 3), -1.2 W m^{-2} for our fixed SST experiments. The geographical distributions are similar, although the magnitude of AF_7 in some regions is smaller, for example, the positive forcing changes in the polar regions and the negative forcing changes over the oceans. Furthermore, approximately the same ACF_7 results from the Qflux experiments, suggesting that global climate feedbacks are small. For the Qflux experiment with increasing GHG, the ACF_7 is only slightly larger, -1.3 W m^{-2} .

Note however, that the IE must be isolated from the DE in order to achieve this equivalency in forcing. Such isolation is artificial, because in the real world the IE does not occur without the DE and the experiments with both DE and IE are most realistic (the central section of Table 3). However, for this case, the TOA flux change AF_{DI} , -1.4 W m^{-2} , is much greater than the ACF_{DI} , -0.6 W m^{-2} . As discussed above, in our model diagnostics the CF_{DI} includes the artificial effect of taking the difference between cloudy conditions and bright aerosol (for pre-

sent day), so that the ACF_{DI} is underestimated. Thus the TOA flux calculation is more realistic. This suggests that CF calculations of the IE must be used carefully, either by isolating the IE parameters, as Rotstajn and Penner (2001) did, or by subtracting the CF_D as we do. Alternatively, the cloud-free condition could also be diagnosed using an aerosol-free atmosphere.

Now we compare our IE forcing with some other recent studies. Our ACF_{DI} value without increasing GHG, -0.62 W m^{-2} , is very similar to that obtained by Menon and Del Genio (2007) (-0.65 W m^{-2}) with a similar model version. Takemura et al. (2005) estimated -0.94 W m^{-2} for first and second IE (using net flux change at TOA). Solomon et al. (2007) made a central estimate of -0.7 W m^{-2} for the albedo (first) IE only. All of these are larger than the estimates of Quaas et al. (2005) (-0.53 W m^{-2}), for simulations constrained with satellite data.

In general, the TOA SW flux change spatial pattern (Fig. 12) is anticorrelated with cloud changes (Fig. 7). This suggests that cloud changes from the aerosol effects impact SAT especially in the shortwave.

Arctic seasonality of SW TOA forcing change (Fig. 13a) is largest during summer and fall, when aerosol direct forcing (AF_D), cloud and cryospheric changes are also largest (e.g., Fig. 6). The anticorrelation of changes in aerosol forcing and SAT seasonality in the Arctic led Shindell (2007) to conclude that the wintertime Arctic temperature effects were due to nonlocal aerosol forcings.

An alternative hypothesis is that local aerosol effects impact local SAT with delayed seasonality. The sign of

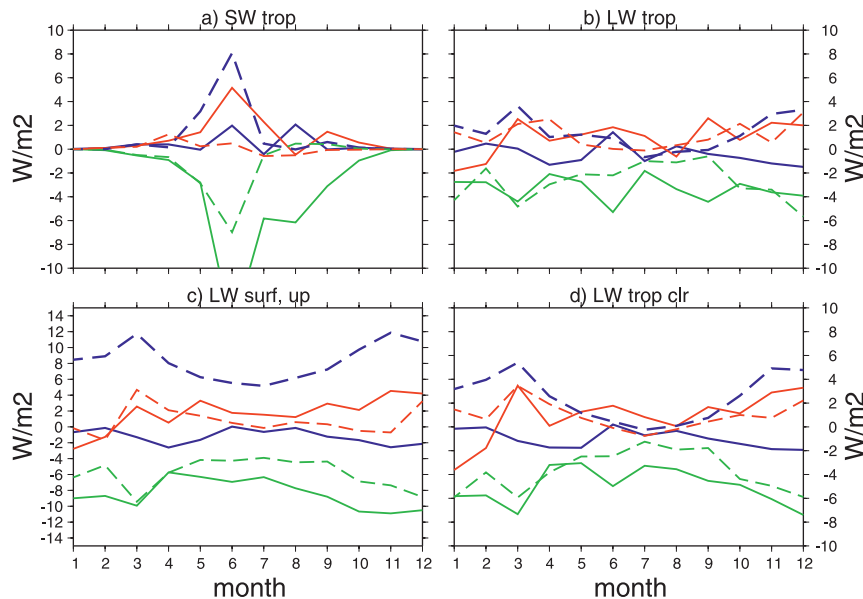


FIG. 13. Monthly Arctic (64° – 90° N) changes in (a) net SW forcing at the tropopause, (b) net LW forcing at the tropopause, (c) LW upward surface forcing, and (d) LW clear-sky forcing at the tropopause, for runs D (blue), Dg (blue dashed), DI-D (green), DIg-Dg (green dashed), DIB-DI (red), and DIBg-DIg (red dashed).

Arctic SAT change (Fig. 6a) is negatively correlated with the sign of the snow/ice cover change (Fig. 6c), although the seasonality differs. Shindell (2007) noted that the DE forcing change is positive in the Arctic even as it cools SAT. However the DE increases snow/ice cover (solid blue, Fig. 6c), mostly over northern Eurasia (Fig. 8a) where cloud cover also increases (Fig. 7a) and temperature reduction is largest (Fig. 5a). The increased snow/ice cover cools ground temperature and changes longwave forcing during winter. Figure 13b shows that the LW forcing change at the tropopause is largest during winter, similar to the SAT seasonality (Fig. 6a). Furthermore, the LW upward forcing change at the surface (Fig. 13c) correlates with the SAT changes (Fig. 6a) and with the ground temperature changes (not shown). Clear-sky forcing changes (Fig. 13d) and seasonal change are larger than all sky (Fig. 13b); thus these longwave forcing changes do not appear to be directly related to cloud changes. Note that the IE on longwave forcing change is negative. Our model does not have an important positive LW cloud forcing change or indirect effect forcing in the Arctic. Presumably this is because the positive LW effect (Garrett and Zhao 2006; Lubin and Vogelmann 2006) occurs for optically thin clouds that are difficult for our model to resolve.

In summary, we suggest that in the Arctic, the aerosol effects change the ice/snow cover during summer and fall, and these cryospheric changes persist to affect wintertime SAT change. The SAT impact may be greater during

winter because of increased atmospheric boundary layer stability. Figure 14 shows zonal mean temperature changes for March and July, two months with large and small Arctic SAT changes (Fig. 6a). The IE temperature impact in the Arctic is confined to the surface during March (Fig. 14d) but significant cooling also occurs aloft in the summer (Fig. 14i). There are also stronger vertical and meridional gradients in temperature change for the BAE in March (Fig. 14e) than in July (Fig. 14j).

Overall, the cooling (aerosol direct and indirect) and warming (GHG and BC–albedo) seasonal effects in the Arctic are generally symmetrical in their influences on radiative forcing (Fig. 13) and on SAT and snow/ice cover (Fig. 6). Forcing and SAT changes, positive or negative, are largest during winter/spring; snow/ice perturbations are largest during summer/fall.

6. Summary and conclusions

We presented equilibrium climate experiments designed to distinguish aerosol direct, indirect, and BC–albedo effects on climate, with and without concurrent GHG changes, over the twentieth century.

We found that the global cooling from aerosol DE and IE is -0.2° and -1.0° C, and the warming from the BAE is about $+0.2^{\circ}$ C over the twentieth century. The net aerosol effect on SAT is approximately half as large and opposite in sign to that of the long-lived GHGs. This is similar to the result of Hansen et al. (2007); Jones et al. (2007) had somewhat smaller aerosol cooling

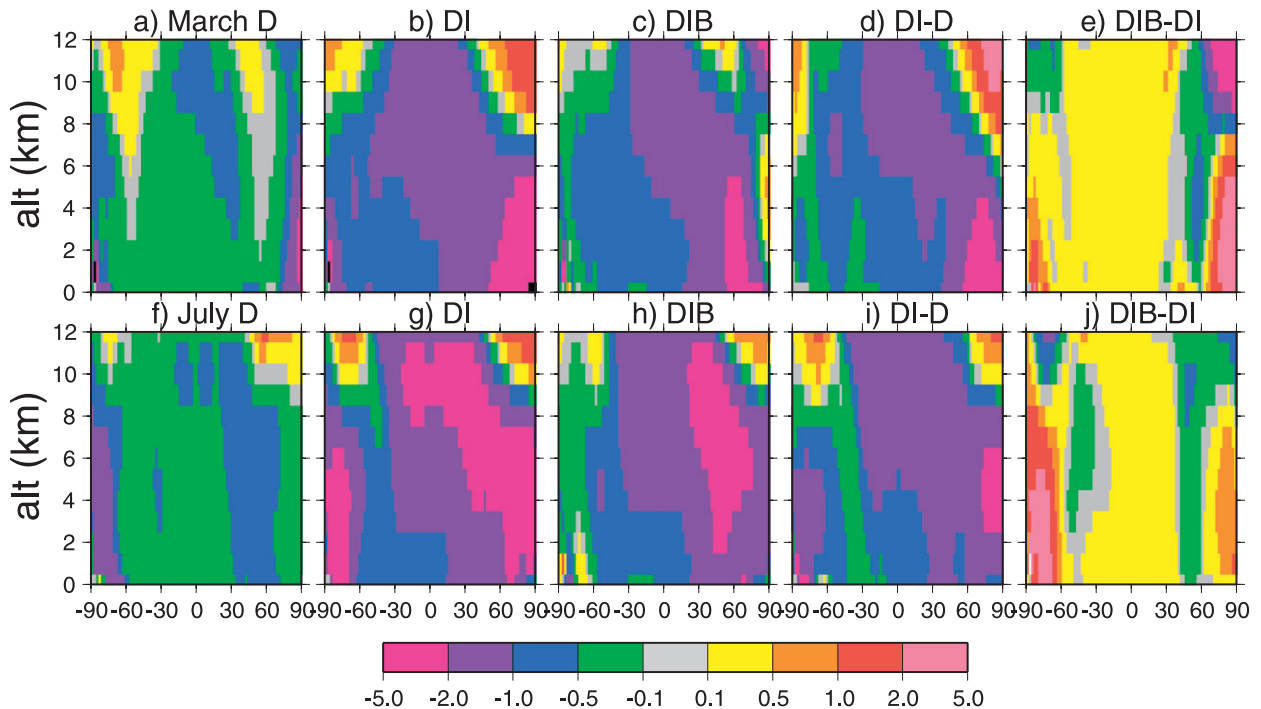


FIG. 14. Zonal mean temperature changes, °C, for (top) March and (bottom) July for (a),(f) DE, (b),(g) DE + IE, (c),(h) DE + IE + BAE, (d),(i) IE, and (e),(f) BAE.

relative to CO₂ warming (ratio of aerosol/GHG SAT effect = -0.3). Our model aerosol cooling effects are larger because of positive feedbacks among clouds, cryosphere, and temperature. Cloud cover increased by 0.1% from the DE and by 0.5% from the IE. Ground albedo increased by 0.01% from the DE, 0.4% from the IE, and -0.1% from the BAE if GHG is constant (these changes are smaller if GHG increase). Thus increased clouds and brighter land surface amplify the aerosol cooling effects.

We explored some of the methods of measuring aerosol IE. A common metric, ACF, is the cloud forcing change (from 1890 to 1995), where the cloud forcing is the change in TOA radiative flux with minus without cloud. Rotstajn and Penner (2001) showed that the ACF agrees with the TOA radiative flux change for the IE for fixed SST conditions. Our analysis agreed, however only if the IE is isolated from the DE. The Rotstajn and Penner (2001) experiments were designed to isolate DE and IE. For our experiments, we had to subtract the DE CF from the DE + IE CF. This is necessary because the CF compares the flux with cloud and without cloud, but the cloud-free condition includes bright aerosols, especially for the present-day calculation. For future studies, we recommend a CF calculation that contrasts the cloudy conditions with a cloud- and aerosol-free condition to remove the aerosol contamination of the

atmosphere without cloud. Our analysis also suggests that the IE forcing from a climate experiment using a Qflux ocean is not very different from the estimate using fixed SSTs. Our IE forcing, -1.2 W m^{-2} , and resulting SAT change are substantial.

Our model BAE also has a relatively large impact on SAT. To understand this and compare with other BAE studies, we consider changes in forcing, albedo, and SAT in Table 5. Comparing ratios of effects helps cancel differences in emissions. One difficulty is that ice/snow cover change, in turn, causes a large forcing change. These responses can vary considerably among models and degree of model equilibrium. The change in albedo from our study is at the low end of the studies in Table 5, the radiative forcing change is also small, and the ratio of forcing to albedo is the smallest, although it is similar to Flanner et al. (2007). The change in SAT per change in albedo ranges from -0.15°C per % (in Jacobson 2004) to -1.5 (in our study), where our study is similar to -1.3°C per % of Hansen and Nazarenko (2004).

Our Arctic surface albedo (and SAT) response is smaller than Flanner et al. (2007); however, our change in Arctic BC is also smaller because of the decreased European BC emissions. Yet within the Arctic, our BAE causes 0.5°C increased SAT and -1.2% decrease in snow/ice cover. These would be even larger if we had used true “preindustrial” or “prehistoric” aerosol

TABLE 5. Comparison of BC–albedo effects with other studies. Sources are BB = biomass burning, FF = fossil fuel, BF = biofuel, 20th century is change during twentieth century, δalb is prescribed albedo change proportional to BC deposition in Koch (2001), ΔF = global mean instantaneous change in forcing from BC–albedo in W m^{-2} , Δalb = global mean change in albedo, %, Δalb_A = Arctic change in albedo, %, ΔSAT = change in SAT, °C. Flanner et al. (2007) show the average of high and low biomass-burning simulations. For Flanner et al. (2007), global albedo change inferred from 0.12 (from NH and this study) \times Arctic albedo, and TOA ΔF inferred from $0.9 \times$ surface forcing.

Study	Source	Δalb	Δalb_A	ΔF	ΔSAT	$\frac{\Delta F}{\Delta\text{alb}}$	$\frac{\Delta\text{SAT}}{\Delta\text{alb}}$
This study	20th century	−0.12	−1.1	0.01	0.18	−0.08	−1.5
Flanner et al. (2007)	BB + FF + BF	−0.40 ⁶	−3.2	−0.045 ⁷	0.12	−0.11	−0.3
Hansen et al. (2005)	δalb	−0.08		0.08	0.05	−1	−0.6
Jacobson (2004)	FF + BF	−0.4		0.06	0.06	−0.15	−0.15
Hansen and Nazarenko (2004)	δalb	−0.19	−1.5	0.16	0.24	−0.84	−1.3

emissions, with zero BC from all industrial activity and biofuel sources. Our results suggest that mitigating Arctic BC sources under present-day GHG conditions should increase snow/ice cover, since this is essentially the reverse of our fixed GHG experiment.

Experiments including concurrent GHG changes generally had smaller aerosol IE and BAE (we do not have an experiment isolating the direct from GHG effects). For example, the IE decreases SAT 20% and snow/ice cover 50% less if GHG also increases. Thus the warming and cooling effects add nonlinearly. The BAE has very small effect on global climate if GHG also increases. Since both act to reduce the snow/ice cover, the incremental effect of the BC–albedo reduction is small, though some regional impacts are evident, such as reduced snow cover in northwestern North America (Fig. 8j). The BAE, with concurrent GHG changes, may be more significant in a transient (rather than equilibrium) simulation. In contrast, global cloud changes are similar with and without GHG changes, although there are regional differences, especially in the Arctic where increasing GHG reduces the CC increase.

In our model, aerosol effects on Arctic climate are large. Our Arctic IE is quite limited because we consider only impacts on liquid clouds; we are currently developing a scheme that includes aerosol effects on ice phase clouds. Similar to other studies, we found largest aerosol effects on clouds and cryosphere during summer–fall with largest SAT effects during winter. The SAT changes correlate with ground temperature and apparently related LW forcing changes. Thus it seems that although aerosol “effects” on Arctic clouds and cryosphere, are maximum in summer–fall, their impact on SAT and sea level pressure persist into winter. We suggest that cryospheric impacts are felt more at the surface more during winter due to increased atmospheric vertical stability in that season.

Future experiments will use transient emissions and climate conditions, a fully coupled ocean, and aerosols and gases fully coupled to the GCM. This will allow study of the evolution of aerosol impacts during the past century.

Acknowledgments. We thank Stephen Warren for assistance in development of the model BC–albedo parameterization. Support for this research is from the Clean Air Task Force, the NASA Radiation Science Program, and the NASA Modeling, Analysis, and Prediction Program.

REFERENCES

- Bond, T. C., D. G. Streets, K. F. Yarber, S. M. Nelson, J.-H. Woo, and Z. Klimont, 2004: A technology-based global inventory of black and organic carbon emissions from combustion. *J. Geophys. Res.*, **109**, D14203, doi:10.1029/2003JD003697.
- , E. Bhardwaj, R. Dong, R. Jogani, S. Jung, C. Roden, D. G. Streets, and N. M. Trautmann, 2007: Historical emissions of black and organic carbon aerosol from energy-related combustion, 1850–2000. *Global Biogeochem. Cycles*, **21**, GB2018, doi:10.1029/2006GB002840.
- Cozic, J., B. Verheggen, S. Mertes, P. Connolly, K. Bower, A. Petzold, U. Baltensperger, and E. Weingartner, 2007: Scavenging of black carbon in mixed phase clouds at the high alpine site Jungfraujoch. *Atmos. Chem. Phys.*, **7**, 1797–1807.
- Davidson, C. I., S. Santhanam, R. C. Fortmann, and M. P. Olson, 1985: Atmospheric transport and deposition of trace elements onto the Greenland ice sheet. *Atmos. Environ.*, **19**, 2065–2081.
- Del Genio, A. D., M.-S. Yao, W. Kovari, and K. K.-W. Lo, 1996: A prognostic cloud water parameterization for global climate models. *J. Climate*, **9**, 270–304.
- , W. Kovari, M.-S. Yao, and J. Jonas, 2005a: Cumulus microphysics and climate sensitivity. *J. Climate*, **18**, 2376–2387.
- , A. B. Wolf, and M.-S. Yao, 2005b: Evaluation of regional cloud feedbacks using single-column models. *J. Geophys. Res.*, **110**, D15S13, doi:10.1029/2004JD005011.
- Feichter, J., E. Roeckner, U. Lohmann, and B. Liepert, 2004: Nonlinear aspects of the climate response to greenhouse gas and aerosol forcing. *J. Climate*, **17**, 2384–2398.
- Flanner, M. G., C. S. Zender, J. T. Randerson, and P. J. Rasch, 2007: Present-day climate forcing and response from black carbon in snow. *J. Geophys. Res.*, **112**, D11202, doi:10.1029/2006JD008003.
- Garrett, T. J., and C. Zhao, 2006: Increased Arctic cloud longwave emissivity associated with pollution from mid-latitudes. *Nature*, **440**, 787–789.
- Hansen, J., and L. Nazarenko, 2004: Soot climate forcing via snow and ice albedos. *Proc. Natl. Acad. Sci. USA*, **101**, 423–428, doi:10.1073/pnas.2237157100.

- , and Coauthors, 2005: Efficacy of climate forcings. *J. Geophys. Res.*, **110**, D18104, doi:10.1029/2005JD005776.
- , and Coauthors, 2007: Climate simulations for 1880–2003 with GISS model E. *Climate Dyn.*, **29**, 661–696, doi:10.1007/s00382-007-02558.
- Harder, S. L., S. G. Warren, R. J. Charlson, and D. S. Covert, 1996: Filtering of air through snow as a mechanism for aerosol deposition to the Antarctic ice sheet. *J. Geophys. Res.*, **101**, 18 729–18 743.
- Haywood, J. M., and V. Ramaswamy, 1998: Global sensitivity studies of the direct radiative forcing due to anthropogenic sulfate and black carbon aerosols. *J. Geophys. Res.*, **103**, 6043–6058.
- Hu, Z. Z., and Z. Wu, 2004: The intensification and shift of the annual North Atlantic Oscillation in a global warming scenario simulation. *Tellus*, **56A**, 112–124.
- Jacobson, M. Z., 2002: Control of fossil-fuel particulate black carbon and organic matter, possibly the most effective method of slowing global warming. *J. Geophys. Res.*, **107**, 4410, doi:10.1029/2001JD001376.
- , 2004: Climate response of fossil fuel and biofuel soot, accounting for soot's feedback to snow and sea ice albedo and emissivity. *J. Geophys. Res.*, **109**, D21201, doi:10.1029/2004JD004945.
- Jones, A., J. M. Haywood, and O. Boucher, 2007: Aerosol forcing, climate response and climate sensitivity in the Hadley Centre climate model. *J. Geophys. Res.*, **112**, D20211, doi:10.1029/2007JD008688.
- Kirchstetter, T. W., T. Novakov, and P. V. Hobbs, 2004: Evidence that the spectral dependence of light absorption by aerosols is affected by organic carbon. *J. Geophys. Res.*, **109**, D21208, doi:10.1029/2004JD004999.
- Koch, D., 2001: Transport and direct radiative forcing of carbonaceous and sulfate aerosols in the GISS GCM. *J. Geophys. Res.*, **106** (D17), 20 311–20 332.
- , G. A. Schmidt, and C. V. Field, 2006: Sulfur, sea salt, and radionuclide aerosols in GISS, ModelE. *J. Geophys. Res.*, **111**, D06206, doi:10.1029/2004JD005550.
- , T. C. Bond, D. Streets, N. Unger, and G. R. van der Werf, 2007: Global impacts of aerosols from particular source regions and sectors. *J. Geophys. Res.*, **112**, D02205, doi:10.1029/2005JD007024.
- Lefohn, A. S., J. D. Husar, and R. B. Husar, 1999: Estimating historical anthropogenic global sulfur emission patterns for the period 1850–1990. *Atmos. Environ.*, **33**, 3435–3444.
- Liu, L., A. A. Lacis, B. E. Carlson, M. I. Mishchenko, and B. Cairns, 2006: Assessing Goddard Institute for Space Studies ModelE aerosol climatology using satellite and ground-based measurements: A comparison study. *J. Geophys. Res.*, **111**, D20212, doi:10.1029/2006JD007334.
- Lohmann, U., and J. Feichter, 2005: Global indirect aerosol effects: A review. *Atmos. Chem. Phys.*, **5**, 715–737.
- Lubin, D., and A. M. Vogelmann, 2006: A climatologically significant aerosol longwave indirect effect in the Arctic. *Nature*, **439**, 453–456.
- Marshall, S. E., 1989: A physical parameterization of snow albedo for use in climate models. Ph.D. thesis, University of Washington, NCAR, and University of Colorado, 161 pp.
- Menon, S., and L. Rotstayn, 2006: The radiative influence of aerosol effects on liquid-phase cumulus and stratiform clouds based on sensitivity studies with two climate models. *Climate Dyn.*, **27**, 345–356, doi:10.1007/s00382-006-0139-3.
- , and A. D. Del Genio, 2007: Evaluating the impacts of carbonaceous aerosols on clouds and climate. *Human-Induced Climate Change: An Interdisciplinary Assessment*, M. Schlesinger et al., Eds., Cambridge University Press, 34–48.
- , —, Y. Kaufman, R. Bennartz, D. Koch, N. Loeb, and D. Orlikowski, 2008: Analyzing signatures of aerosol-cloud interactions from satellite retrievals and the GISS GCM to constrain the aerosol indirect effect. *J. Geophys. Res.*, **113**, D14S22, doi:10.1029/2007JD009442.
- Noone, K. J., and A. D. Clarke, 1988: Soot scavenging measurements in Arctic snowfall. *Atmos. Environ.*, **22**, 2773–2778.
- Penner, J. E., C. C. Chuang, and K. Grant, 1998: Climate forcing by carbonaceous and sulfate aerosols. *Climate Dyn.*, **14**, 839–851.
- Proshutinsky, A. Y., and M. A. Johnson, 1997: Two circulation regimes of the wind-driven Arctic Ocean. *J. Geophys. Res.*, **102** (C6), 12 493–12 514.
- Quaas, J., O. Boucher, and U. Lohmann, 2005: Constraining the total aerosol indirect effect in the LMDZ and ECHAM4 GCMs using MODIS satellite data. *Atmos. Chem. Phys.*, **5**, 9669–9690.
- Rind, D., J. Perlwitz, P. Lonergan, and J. Lerner, 2005: AO/NAO response to climate change: 2. Relative importance of low- and high-latitude temperature changes. *J. Geophys. Res.*, **110**, D12108, doi:10.1029/2004JD005686.
- Romanou, A., B. Liepert, G. A. Schmidt, W. B. Rossow, R. A. Ruedy, and Y. Zhang, 2007: 20th century changes in surface solar irradiance in simulations and observations. *Geophys. Res. Lett.*, **34**, L05713, doi:10.1029/2006GL028356.
- Rotstayn, L. D., and J. E. Penner, 2001: Indirect aerosol forcing, quasi-forcing, and climate response. *J. Climate*, **14**, 2960–2975.
- Schmidt, G. A., and Coauthors, 2006: Present day atmospheric simulations using GISS ModelE: Comparison to in situ, satellite, and reanalysis data. *J. Climate*, **19**, 153–192.
- Schulz, M., and Coauthors, 2006: Radiative forcing by aerosols as derived from the AeroCom present-day and pre-industrial simulations. *Atmos. Chem. Phys.*, **6**, 5225–5246.
- Shindell, D., 2007: Local and remote contributions to Arctic warming. *Geophys. Res. Lett.*, **34**, L14704, doi:10.1029/2007GL030221.
- , R. L. Miller, G. A. Schmidt, and L. Pandolfo, 1999: Simulation of recent northern winter climate trends by greenhouse-gas forcing. *Nature*, **399**, 452–455.
- Sigmund, M., P. C. Siegmund, E. Manzini, and H. Kelder, 2004: A simulation of the separate climate effects of middle-atmosphere and troposphere CO₂ doubling. *J. Climate*, **17**, 2352–2367.
- Solomon, S., D. Qin, M. Manning, M. Marquis, K. Averyt, M. M. B. Tignor, H. L. Miller Jr., and Z. Chen, Eds., 2007: *Climate Change 2007: The Physical Science Basis*. Cambridge University Press, 996 pp.
- Takemura, T., T. Nozawa, S. Emori, T. Y. Nakajima, and T. Nakajima, 2005: Simulation of climate response to aerosol direct and indirect effects with aerosol transport-radiation model. *J. Geophys. Res.*, **110**, D02202, doi:10.1029/2004JD005029.
- van Aardenne, J. A., F. J. Dentener, J. G. J. Olivier, C. G. M. K. Goldewijk, and J. Lelieveld, 2001: A 1° × 1° resolution dataset of historical anthropogenic trace gas emissions for the period 1890–1990. *Global Biogeochem. Cycles*, **15**, 909–928.
- Wang, C., 2004: A modeling study on the climate impacts of black carbon aerosols. *J. Geophys. Res.*, **109**, D03106, doi:10.1029/2003JD004084.
- Warren, S. G., and W. J. Wiscombe, 1985: Dirty snow after nuclear war. *Nature*, **313**, 467–470.
- , I. G. Rigor, N. Untersteiner, V. F. Radionov, N. N. Briazgin, Y. I. Aleksandrov, and R. Colony, 1999: Snow depth on Arctic sea ice. *J. Climate*, **12**, 1814–1829.
- Yao, M.-S., and A. D. Del Genio, 1999: Effects of cloud parameterization on the simulation of climate changes in the GISS GCM. *J. Climate*, **12**, 761–779.